Road Code Marking-Assisted Localization for Autonomous Vehicles in Tunnels

Yaoli Shi, Zhiguo Zhao, *Member, IEEE,* Danshu Yan and Yifei Yang

***Abstract*— Accurate vehicle localization in tunnels is challenging due to limited global navigation satellite system (GNSS) signals and degenerated structures. To address this problem, this paper proposes a road code marking-assisted localization method, which provides vehicles with accurate positional information through specially designed road code markings embedded with encoding coordinates in tunnels. First, a novel encoding scheme is designed, embedding centimeter-level positioning coordinates into road code markings. To overcome low-light conditions in tunnels, an adaptive intensity adjustment algorithm is applied as a preprocessing step to dynamically optimize image contrast before detection. A detection network leveraging geometric pattern constraints is then developed, achieving real-time inference at 45 Hz. After decoding and verification, precise positioning information is recovered. Experimental results show that one road code marking can be successfully decoded at least three times (at 70-80 km/h). In field tests over a 260-meter road segment, the proposed method reduced the average localization error from 7.71 meters to 0.31 meters. This work represents a practical and cost-effective solution for high-precision localization in tunnels.**

I. Introduction

Accurate vehicle localization serves as the cornerstone of autonomous driving systems, directly influencing path planning, control and operational safety. As automation levels increase [1], the demands for localization accuracy and reliability become increasingly stringent, particularly in global navigation satellite system (GNSS)-degraded environments. Tunnels play a vital role in modern transportation networks, enabling efficient and uninterrupted travel. However, GNSS-based localization, which provides centimeter-level accuracy in open environments, becomes unreliable in tunnels due to signal obstruction and multipath effects. Therefore, improving localization accuracy and reliability in GNSS-denied tunnel environments remains an urgent research priority.

Existing localization approaches in GNSS-denied environments can be broadly categorized into three main types: sensor-based approaches, Vehicle-to-Everything (V2X)-based approaches, and map-based techniques. Sensor-based methods rely on onboard sensors such as Inertial Measurement Units (IMUs), wheel encoders, LiDARs and cameras to estimate vehicle motion through dead reckoning (DR) or Simultaneous Localization and Mapping (SLAM). IMUs and wheel encoders are commonly used in DR systems, which provide short-term positioning but suffer from cumulative drift, requiring periodic corrections [2], [3], [4]. LiDAR and visual SLAM reconstruct tunnel structures for localization, achieving high accuracy in structured environments. However, the highly repetitive and texture-less nature of tunnel interiors reduces the robustness of SLAM-based approaches, making them unreliable in such scenarios [5].

With the development of Vehicle-to-Everything (V2X) technology, V2X-based localization has emerged as a potential solutions for tunnels [6], [7]. These methods determine the vehicle's position through wireless communication with other vehicles (V2V) or infrastructure (V2I) using technologies such as Bluetooth Low Energy (BLE) [8], Wi-Fi [9], Ultra-Wideband (UWB) [10] and Radio-Frequency Identification (RFID)[11]. However, the accuracy of V2X-based localization largely hinges on the density and quality of communication devices. The high deployment and maintenance costs of V2X systems pose significant challenges for large-scale adoption, limiting their feasibility as a universal solution in tunnels [5].

Map-based localization relies on pre-constructed high-definition maps to match real-time sensor data. Some studies have leveraged pole-like landmarks such as trees and streetlights for accurate localization [12], but their applicability is significantly constrained by the availability of landmarks. Lane markings have gained attention due to their widespread presence [13], [14]. Kim et al. [15] proposed a 3D LiDAR-based method that matches vehicle observations with tunnel infrastructure, achieving real-time decimeter-level localization, but its accuracy depends on the completeness of tunnel facilities. Niu et al. [16] formulated lateral vehicle-to-lane distances obtained from cameras into constraints and matched them with a lane-level map to constrain lateral positioning errors, yet this method lacks the capability to refine longitudinal positioning. Kang et al. [17] integrated lane centerline information from maps with GPS trajectories and applied the iterative closest point algorithm to minimize localization errors, achieving lane-level accuracy in highway and urban scenarios. While these methods work well in environments with abundant and distinguishable features, their applicability is significantly limited in tunnels, where feature points and pavement markings are often sparse and repeated, making robust map-matching difficult and reducing localization accuracy.

To bridge this gap, some researchers have explored embedding positional information into existing road markings or designing novel road markings to support vehicle localization. Tao et al. [18] encoded positional data into lane lines using yellow and white patterns and achieved sub-meter

Research supported by the National Key Research and Development Program of China (No.2023YFE0202400) and the National Natural Science Foundation of China (No.52172390). (Corresponding author: Zhiguo Zhao.)

Yaoli Shi, Zhiguo Zhao, Danshu Yan and Yifei Yang are with the School of Automotive Studies, Tongji University, Shanghai 201804, China (e-mail: 2332878@tongji.edu.cn; zhiguozhao@tongji.edu.cn; 2311386@tongji.edu.cn; 1652083@tongji.edu.cn).

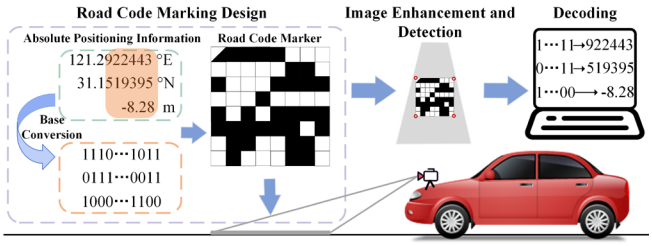

Figure 1. Framework of the road code marking-assisted localization method.

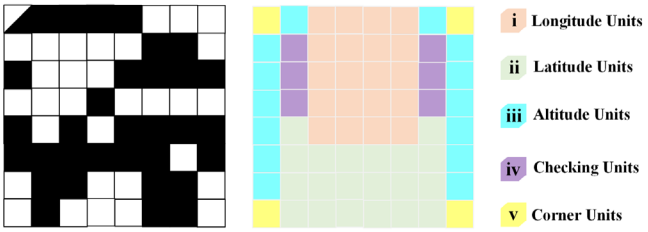

Figure 2. Example of a road code marking.

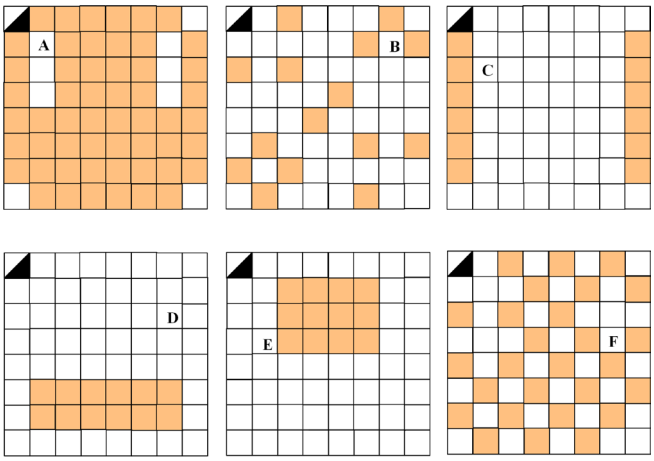

Figure 3. Checking regions.

accuracy. But its simplistic encoding limited broader applicability. Wang et al. [19] developed a pavement marking embedded with localization information, which can be detected by onboard vehicle cameras and decoded. However, its effectiveness was restricted by its visual interference, suboptimal detection and decoding robustness, and inability to provide continuous positioning. In our previous work [20], we implemented a vehicle-road cooperative localization approach that continuously provided high-precision positioning. However, the method struggled in tunnels due to low lighting conditions, where detection performance deteriorated significantly. Additionally, the limited information capacity of the markings only allowed for error corrections at meter-to-centimeter levels, which is insufficient in tunnels where GNSS signals are completely unavailable, potentially leading to errors exceeding ten meters between two markings.

Overall, the repetitive structure, sparse distinguishable features, and GNSS unavailability in tunnels make traditional localization methods challenging. Given that tunnel environments have stable lighting and are unaffected by adverse weather, road code marking-based localization is a viable alternative. This paper proposes a low-cost road code marking-assisted localization method specifically designed for tunnels (Fig. 1). A novel marking design is introduced, encoding positional data with kilometer-to-centimeter precision to provide accurate absolute positioning. To enhance detection robustness in low-light conditions, an adaptive image enhancement algorithm and a geometric-prior-based detection network are developed. The proposed method offers a reliable and high-precision localization solution, effectively mitigating cumulative errors and ensuring continuous positioning support for autonomous vehicles in tunnels.

The structure of the paper is as follows: Section II introduces the design of the road code marking. Section III details the detection and decoding methods developed for the marking. Section IV presents experimental validations of the developed method. Finally, Section V concludes the paper.

II. Road Code Marking Design

In the proposed method, road code markings provide high-precision positional data to correct errors in other localization methods, such as odometry, ensuring accurate positioning in tunnels. This section presents the design of the road code marking. As shown is Fig. 2, the marking encodes global positional information into a compact 8×8 black-and-white grid, which can be directly painted on the road surface with minimal spatial footprint. Each 0.06 m × 0.06 m cell represents a single bit of data, categorized into three functional types: encoding units, checking units, and corner units.

A. Encoding Units

Encoding units store longitude, latitude, and altitude information using a reduced-digit representation based on the WGS-84 coordinate system. Considering that the first few digits of longitude and latitude usually remain constant between adjacent markings, only the key digits—2nd to 7th decimal for longitude and latitude (covering kilometer-to-centimeter scales) and integer to hundredth decimal for altitude—are encoded, requiring 20 bits for longitude, 20 for latitude, and 14 for altitude, which can balance precision and efficiency well. The binary sequence is arranged from left to right and top to bottom, with black denoting 1 and white denoting 0. For example, the encoded values in Fig. 2 are as follows: longitude "11100001001101001011" (corresponding to a decimal value of 922443), latitude "519395," and altitude "-8.28."

B. Checking Units

To enhance decoding reliability, six checking units perform parity checks on different encoding regions (Fig. 3). Region A verifies all encoding cells, while regions B and F detect local errors from lighting variations. Edge regions C and D check perspective distortion, and region E focuses on occlusions or wear. This multi-layered error-checking mechanism improves robustness against environmental interference.

C. Corner Units

Corner units, positioned at the four vertices, assist in initial detection and orientation. Unlike previous designs using colored markers, which introduced distractions and sensitivity

to lighting, this study employs a black-and-white scheme to maintain consistency and minimize visual interference. The proposed detection network directly identifies corner units without relying on color filtering, enhancing adaptability and accuracy.

III. Road Code Marking Detection and Decoding

Autonomous vehicle cameras capture road code markings along with lane markings and road surfaces. The proposed vision-aided localization method relies on real-time detection and decoding of these markings to extract precise positional data. This section introduces an image enhancement algorithm designed to improve detection under low-light tunnels, a corner detection network leveraging the geometric priors of road code markings, and a decoding strategy for processing the detection results.

A. Image Enhancement

Low illumination in tunnels poses challenges for detecting road code markings. While increasing the camera's exposure time can improve brightness, it also introduces motion blur at high speeds, which compromises detection accuracy. Experimental results indicate that a 2 ms exposure time effectively minimizes motion blur even at 80 km/h, but it results in low brightness and contrast. In practice, without image enhancement, the detection and decoding of road code markings consistently failed under such low-light conditions. To overcome this issue, a locally adaptive image enhancement algorithm is employed. Rather than uniformly increasing brightness, the method selectively enhances the contrast between road code markings and the pavement background, highlighting critical structural features for corner detection. The enhancement process is illustrated in Fig. 4.

1) Shadow Region Segmentation

To enhance contrast in low-light conditions, the input RGB image is first converted into a grayscale image, and its mean grayscale value is computed as a global lighting reference. Based on this reference, a threshold is set to classify regions: pixels with values below the threshold are identified as shadowed regions, while the remaining areas are labeled as non-shadowed. A binary mask is generated, where shadowed regions are marked as 0 and non-shadowed regions as 255. This segmentation enables subsequent adaptive contrast adjustments tailored to different regions.

2) Adaptive Contrast Adjustment

Contrast is adjusted using an exponential transformation:

$$s = r^{c} \tag{1}$$

where r and s are the original and enhanced pixel values, respectively, and c controls the degree of enhancement. For $c<1$, contrast in shadowed regions is enhanced, while $c>1$ strengthens bright areas. Different values of c are applied to shadowed and non-shadowed regions to prevent over-enhancement. The c follows:

$$c = \begin{cases} c_1 & mask = 0 \\ c_2 = \dfrac{log(1+ar)}{log(1+r)} & mask = 255 \end{cases} \tag{2}$$

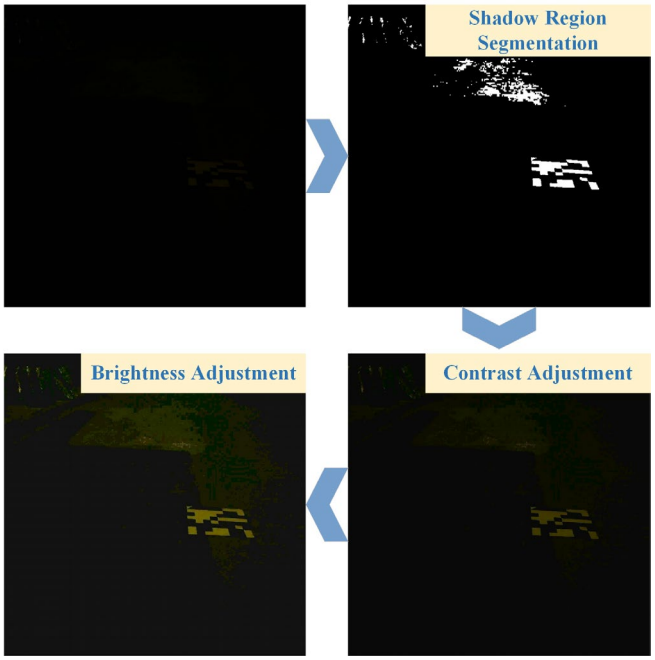

Figure 4. Workflow of the image enhancement process.

where c_1 is fixed for improving shadowed regions, a is an empirical value based on light conditions, and c_2 dynamically adjusts based on pixel intensity to ensure smooth transitions. This adaptive approach effectively improves image contrast, accentuating critical details in road code markings.

3) Brightness Adjustment

After contrast enhancement, the overall brightness of the image is further improved using a nonlinear scaling function:

$$s = -r^2 + 2r \tag{3}$$

This function smoothly increases the brightness while avoiding overexposure, ensuring a more uniform brightness distribution. As shown in Fig. 4, the enhanced image exhibits higher contrast and brightness, enabling robust detection and decoding in low-light conditions.

B. Road Code Marking Detection

Real-time detection of road code markings requires both high accuracy and efficiency. Traditional methods such as edge detection struggle with robustness under varying lighting conditions and occlusions, making it difficult to precisely locate corners, which in turn affects decoding accuracy. Consequently, this study proposes a lightweight single-stage detection network specifically designed to detect the four corners of road code markings in real time.

The network processes a 416×416 RGB image and outputs a 3×26×26 tensor, dividing the image into a 26×26 grid. Each grid cell predicts the confidence score and the horizontal and vertical offsets of a corner point relative to the top-left corner. The backbone network employs ResNet18 [21] for feature extraction. To enhance feature localization, a Convolutional Block Attention Module (CBAM) is integrated, refining feature maps through channel and spatial attention

mechanisms. Additionally, a Spatial Pyramid Pooling (SPP) layer improves scale robustness by performing multi-kernel max pooling. The head network consists of 5 convolutional layers that progressively refine features, reducing dimensionality to generate confidence scores and offset predictions for each grid cell.

In traditional corner detection methods, they usually optimize confidence and position metrics alone, and the influence of edge geometry on corner localization is not considered. For road code markings, the corners correspond to the intersections of boundary edges, making edge features critical for accurate corner detection. Based on this, we propose a composite loss that explicitly utilizes the structural prior of road code markings. The loss function introduces edge geometry regularization as a third constraint term, guiding the network to focus on structural features without additional computational overhead. The overall loss function consists of confidence loss L_{conf}, corner position loss L_{pos}, and edge loss L_{edge}, formulated as:

$$L = \alpha L_{conf} + \beta L_{pos} + \gamma L_{edge} \tag{4}$$

where α, β, and γ are empirically determined weight coefficients.

The confidence loss measures the discrepancy between predicted and ground truth confidence scores. It is calculated as:

$$L_{conf} = \sum_{i=1}^{26^2} (conf_i - \widehat{conf_i})^2 \tag{5}$$

where $conf_i$ is the predicted confidence score for grid i, and $\widehat{conf_i}$ is the corresponding ground truth confidence.

The corner position loss L_{pos} quantifies the deviation between the predicted offsets and the ground truth values, ensuring precise corner localization. It is defined as:

$$L_{pos} = \sum_{i=1}^{26^2} (\widehat{conf}_i)\left((tx_i - \widehat{tx_i})^2 + (ty_i - \widehat{ty_i})^2\right) \tag{6}$$

where tx_i and ty_i represent the predicted offsets in the horizontal and vertical directions for grid i, $\widehat{tx_i}$ and $\widehat{ty_i}$ are the corresponding ground truth offsets.

Edge loss L_{edge} comprises length loss and angle loss. Length loss optimizes the structure of the marking by minimizing the difference between the predicted and true edge lengths. Angle loss ensures consistency in the direction of corner-connected edges by constraining their sine and cosine values. The combined edge loss is expressed as:

$$L_{edge} = \sum_{i=1}^{n} (l_i - \hat{l}_i)^2 + (cos\theta_i - cos\widehat{\theta}_i)^2 + (sin\theta_i - sin\widehat{\theta}_i)^2 \tag{7}$$

where n is the number of edges associated with the corners in the image, l_i and $\hat{l}_i$ are the predicted and ground truth edge lengths, and θ_i, $\widehat{\theta}_i$ are the predicted and ground truth angles, respectively.

We deployed road code markings in tunnel environments and collected 812 images using a forward-facing onboard camera. Of these, 122 images were used for testing, while the remaining 690 were split into training and validation sets. Data augmentation techniques, including image flipping and random color adjustments, were applied to improve network robustness. Training was conducted on a system with an AMD R9-7945HX processor, an RTX 4060 GPU, and 8GB of memory. The trained network contains 12.43M parameters, has a FLOP count of 24.68B, and achieves real-time inference at 45 Hz.

The network without edge loss achieved an accuracy of 98.64%, a recall of 91.88%, and an average corner coordinate error of 4.76 pixels. With edge loss incorporated, accuracy slightly increased to 98.67%, recall improved to 94.44%, and the average corner coordinate error was reduced to 4.21 pixels, representing an 11.55% reduction. The results demonstrate that edge loss enhances the network's ability to capture the geometric features of road code markings, improving detection robustness in low-light tunnel environments. As a result, the trained network reliably detects marking corners in tunnels with high accuracy and stability.

C. Decoding Methodology

After detecting the road code marking, accurately decoding the embedded information is a critical task for the system. An efficient and precise decoding process is developed to extract and restore the information from the road code marking. As illustrated in Fig. 5, the decoding process consists of the following four steps:

1) Inverse Perspective Mapping (IPM)

Perspective distortion causes the road code marking to appear deformed in the captured image, reducing decoding accuracy. To correct this, IPM is applied using the four detected corner points to estimate a perspective transformation matrix $\mathbf{H}$, which maps each pixel to its original square geometry:

$$\mathbf{p}' = \mathbf{H} \cdot \mathbf{p} \tag{8}$$

where $\mathbf{p}$ and $\mathbf{p}'$ are the original and target image coordinates, respectively. This correction restores geometric accuracy for subsequent processing.

2) Image Binarization

The rectified image may still be affected by lighting or noise, hindering information extraction. To improve robustness, Otsu thresholding method [22] is applied, adaptively determining the optimal threshold to separate black and white regions, ensuring clear distinction for information parsing.

3) Information Parsing

The binarized image is then divided into an 8×8 grid corresponding to the marking's structure. Each cell's black

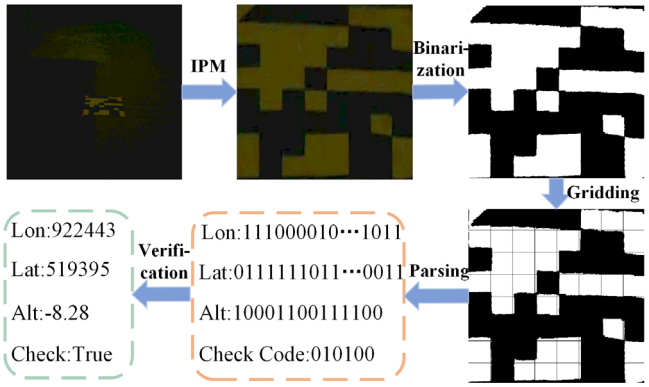

Figure 5. Workflow of the decoding algorithm.

pixel ratio p is computed, and the predefined threshold t determines whether it is classified as black (1) or white (0). This process converts the visual pattern into an 8×8 binary matrix, which is then reorganized into a continuous sequence based on a predefined scanning order.

4) Verification and Conversion

The extracted binary sequence undergoes verification by checking parity values against predefined check regions. If all checks pass, the binary data is converted into decimal coordinates; otherwise, the result is discarded to maintain accuracy. This mechanism enhances reliability by mitigating errors caused by environmental interference, marking degradation, or detection inaccuracies, ensuring robust localization and information transmission.

IV. Road Tests

To evaluate the detection and decoding performance of the system, a road code marking was placed at the road center, ensuring stable image capture at different vehicle speeds. The test vehicle, equipped with an MV-SUF401GC/GM high-speed camera operating at 60 Hz, was precisely adjusted to maintain clear visibility of the marking within the camera's field of view. Vehicle speeds ranged from 10 to 80 km/h, divided into seven intervals. For each speed interval, two trials were conducted, and the average number of successfully detected and decoded frames per marking at each speed was recorded as the marking entered and exited the camera's line of sight.

As shown in Table I, the system successfully decoded an average of 24 frames per marking at 10–20 km/h. As vehicle speed increased, the number of decoded frames gradually decreased due to reduced dwell time and increased motion blur, which impacted detection and decoding accuracy. Nevertheless, even at high speeds of 70–80 km/h, the system still decoded an average of three frames per marking, demonstrating its robustness against increased motion blur at higher vehicle speeds.

It is noteworthy that during the marking's presence within the camera's field of view (approximately 5 meters in the test), a single successful decoding is sufficient to provide high-precision positional information for correcting global localization errors. At 80km/h speeds, where the marking was visible for only about 0.2 seconds, the cumulative errors of other localization methods (e.g., odometry) remains limited,

TABLE I. Average Number of Detetion and Decoding Frames

Vehicle speed(km/h)	*Detection frames*	*Correctly decoding frames*
10-20	26	24
20-30	16	15
30-40	13	11
40-50	9	6
50-60	7	5
60-70	7	5
70-80	4	3

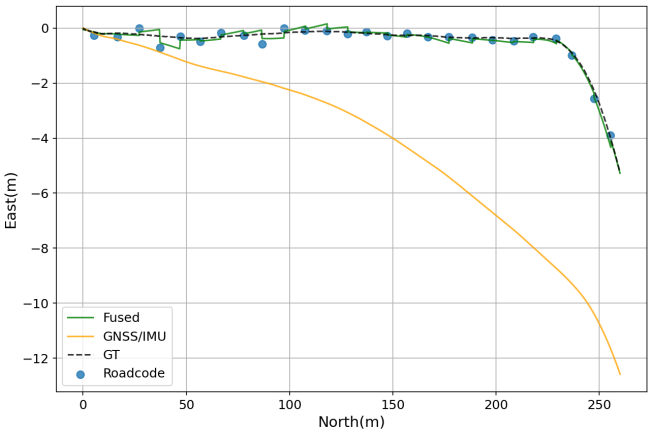

Figure 6. Localization performance assisted by road code markings.

reducing the required correction frequency. Thus, despite fewer decoded frames at 80km/h speeds, the system effectively supported auxiliary localization.

To evaluate the localization effectiveness of the presented approach, a field test was conducted on a 260-meter road segment where 26 road code markings were evenly placed at 10-meter intervals. Since obtaining ground truth trajectory data in real tunnels is impractical, experiments were conducted on a campus road where the RTK module provided reference positioning. To simulate GNSS-denied tunnel conditions, GNSS signals were manually disabled after the initial frames. The test vehicle was equipped with a GNSS/IMU integrated navigation system, a high-speed camera, an industrial computer for real-time algorithm execution, and an RTK module. Consistent with our previous study [20], the localization information derived from road code markings was fused with the GNSS/IMU system using an Error State Kalman Filter.

Fig. 6 illustrates the localization performance with and without the assistance of road code markings. When GNSS signals were unavailable, the GNSS/IMU system's trajectory gradually deviated from the ground truth as the vehicle traveled further. This drift resulted from the IMU's reliance on local pose estimation without global updates, leading to cumulative localization errors. Over the 260-meter trajectory, the GNSS/IMU-only solution yielded an average localization error of 7.71 meters and a root mean square error (RMSE) of 9.99 meters, highlighting its limitations in GNSS-denied environments. In contrast, the integration of road code markings significantly improved positioning accuracy, achieving an average error of 0.31 meters and an RMSE of

0.34 meters. The precise yet low-frequency localization data from road code markings effectively corrected the cumulative drift errors of the GNSS/IMU system, significantly enhancing localization accuracy and reliability. These results suggest that the proposed road code marking-based localization method is a practical and effective auxiliary solution for high-precision vehicle localization in tunnels.

V. Conclusion

This paper develops a road code marking-assisted localization method for vehicles in tunnels. A novel road code marking design is introduced, encoding positional data with kilometer-to-centimeter precision to provide absolute localization. An adaptive image enhancement algorithm is implemented, which improves detection under low-light conditions. A unified detection and decoding algorithm achieves robust corner detection at 45 Hz and ensures reliable information extraction. Experimental results demonstrate that the proposed method enables accurate detection and decoding of road code markings at speeds up to 80 km/h. When integrated with GNSS/IMU data, it effectively corrects localization drift, reducing average positioning error from 7.71 meters to 0.31 meters. These results confirm the method's capability to provide stable, high-precision positioning for autonomous vehicles in tunnels.

While the proposed method enhances localization accuracy and reliability in tunnels, its performance may be affected by marking wear or occlusion, potentially limiting long-term reliability. Additionally, despite efforts to minimize visual interference, the markings remain visible to drivers. Future research will explore more durable and less intrusive encoding formats, such as infrared-coded markings, to improve resilience against environmental factors while maintaining high localization accuracy.

References

[1] O.-R. A. D. (ORAD) Committee, Taxonomy and definitions for terms related to driving automation systems for on-road motor vehicles. SAE International, 2021.

[2] Y. Zhuang et al., "Multi-sensor integrated navigation/positioning systems using data fusion: From analytics-based to learning-based approaches," Information Fusion, vol. 95, pp. 62–90, 2023, doi: 10.1016/j.inffus.2023.01.025.

[3] E. Javanmardi, Y. Gu, M. Javanmardi, and S. Kamijo, "Autonomous vehicle self-localization based on abstract map and multi-channel LiDAR in urban area," IATSS research, vol. 43, no. 1, pp. 1–13, 2019.

[4] Q. Lou, F. Gonzalez, and J. Kovecses, "Kinematic Modeling and State Estimation of Exploration Rovers," IEEE Robotics and Automation Letters, vol. PP, no. 99, pp. 1–1, 2019.

[5] Q. Tao, Z. Hu, Y. Liu, and Z. Zhu, "LiDAR-Based Localization in Tunnel From HD Map Matching With Pavement Marking Likelihood," IEEE Transactions on Instrumentation and Measurement, vol. 73, 2024, doi: 10.1109/TIM.2024.3411138.

[6] Y. Lu, H. Ma, E. Smart, and H. Yu, "Real-time performance-focused localization techniques for autonomous vehicle: A review," IEEE Transactions on Intelligent Transportation Systems, vol. 23, no. 7, pp. 6082–6100, 2021.

[7] L. Gao, H. Xiang, X. Xia and J. Ma, "Multisensor Fusion for Vehicle-to-Vehicle Cooperative Localization With Object Detection and Point Cloud Matching," in IEEE Sensors Journal, vol. 24, no. 7, pp. 10865-10877, 1 April1, 2024.

[8] M. L. Sollie, K. Gryte, T. H. Bryne, and T. A. Johansen, "Outdoor navigation using Bluetooth angle-of-arrival measurements," IEEE Access, vol. 10, pp. 88012–88033, 2022.

[9] T. Tonggoed and S. Panjan, "Autonomous guided vehicles with wi-fi localization for smart factory," in 2022 7th International Conference on Robotics and Automation Engineering (ICRAE), IEEE, 2022, pp. 70–74.

[10] R. Wang, C. Xu, R. Li, S. Duan and X. Zhang, "Cooperative Localization and Mapping Based on UWB/IMU Fusion Using Factor Graphs," in IEEE Sensors Journal, vol. 24, no. 14, pp. 21931-21940, 15 July15, 2024.

[11] C. Wu, Z. Gong, B. Tao, K. Tan, Z. Gu, and Z.-P. Yin, "Rf-slam: Uhf-rfid based simultaneous tags mapping and robot localization algorithm for smart warehouse position service," IEEE Transactions on Industrial Informatics, vol. 19, no. 12, pp. 11765–11775, 2023.

[12] Q. Tao, Z. Hu, Y. Liu, and Z. Zhu, "LiDAR-Based Localization in Tunnel From HD Map Matching With Pavement Marking Likelihood," Transactions on Instrumentation and Measurement, vol. 73, 2024, doi: 10.1109/TIM.2024.3411138.

[13] L. Deng, M. Yang, B. Hu, T. Li, H. Li, and C. Wang, "Semantic segmentation-based lane-level localization using around view monitoring system," IEEE Sensors Journal, vol. 19, no. 21, pp. 10077–10086, 2019.

[14] K.-W. Kim and G.-I. Jee, "Free-resolution probability distributions map-based precise vehicle localization in urban areas," Sensors, vol. 20, no. 4, p. 1220, 2020.

[15] K. Kim, J. Im, and G. Jee, "Tunnel Facility Based Vehicle Localization in Highway Tunnel Using 3D LIDAR," IEEE transactions on intelligent transportation systems, vol. 23, no. 10, pp. 17575–17583, 2022.

[16] X. Niu, Y. Peng, Y. Dai, Q. Chen, C. Guo and Q. Zhang, "Camera-Based Lane-Aided Multi-Information Integration for Land Vehicle Navigation," in IEEE/ASME Transactions on Mechatronics, vol. 28, no. 1, pp. 152-163, Feb. 2023, doi: 10.1109/TMECH.2022.3192985.

[17] J. M. Kang, T. S. Yoon, E. Kim, and J. B. Park, "Lane-level map-matching method for vehicle localization using GPS and camera on a high-definition map," Sensors, vol. 20, no. 8, p. 2166, 2020.

[18] Q. Tao, Z. Hu, H. Cai, G. Huang, and J. Wu, "Coding pavement lanes for accurate self-localization of intelligent vehicles," in 2018 IEEE Intelligent Vehicles Symposium (IV), IEEE, 2018, pp. 1458–1463.

[19] Y. Wang, Y. Wang, I. W.-H. Ho, W. Sheng, and L. Chen, "Pavement Marking Incorporated With Binary Code for Accurate Localization of Autonomous Vehicles," IEEE Trans. Intell. Transport. Syst., vol. 23, no. 11, pp. 22290–22300, Nov. 2022, doi: 10.1109/TITS.2022.3173656.

[20] Y. Yang, Z. Zhao, D. Yan, Y. Wang and X. Zhu, "Vehicle-Road Cooperative Positioning Algorithm Based on Road Code in GNSS-Denied Environment," in IEEE Transactions on Intelligent Transportation Systems, vol. 26, no. 4, pp. 5182-5195, April 2025, doi: 10.1109/TITS.2025.3530690.

[21] K. He, X. Zhang, S. Ren, and J. Sun, "Deep residual learning for image recognition," in Proceedings of the IEEE conference on computer vision and pattern recognition, 2016, pp. 770–778.

[22] N. Otsu and others, "A threshold selection method from gray-level histograms," Automatica, vol. 11, no. 285–296, pp. 23–27, 1975.